remote sensing

Article

The Short-Arc Precise Orbit Determination of GEO Satellites Using VLBI and Transfer Ranging

Kai Nan [1,2,3,*], Fen Cao [1,2,3], Jianjun Gong [1,2,3], Hui Lei [1,2,3], Zhigang Li [1,2,3] and Xuhai Yang [1,2,3]

[1] National Time Service Center, Chinese Academy of Sciences, Xi'an 710600, China; caofen@ntsc.ac.cn (F.C.); gongjj@ntsc.ac.cn (J.G.); leihui@ntsc.ac.cn (H.L.); lizhigang@ntsc.ac.cn (Z.L.); yyang@ntsc.ac.cn (X.Y.)
[2] University of Chinese Academy of Sciences, Beijing 100049, China
[3] Key Laboratory of Precise Positioning and Time Technology, Chinese Academy of Sciences, Xi'an 710600, China
* Correspondence: nankai@ntsc.ac.cn

Abstract: It is important for a geostationary Earth orbit (GEO) satellite to rapidly recover its orbit after a maneuver with short-arc precise orbit determination (POD). Based on orbit determination by transfer tracking (ODTT), the POD accuracy of a GEO satellite is less than 10 m over a short arc. ODTT can achieve high accuracy in the radial direction but is weak in the transverse direction. Considering that very long baseline interferometry (VLBI) can reduce the value of position dilution of precision (PDOP), especially in the transverse direction, a joint POD method using both VLBI and ODTT is proposed herein to improve POD accuracy and rapidly recover the orbit. An ODTT system and the first VLBI 2010 Global Observation System (VGOS) in China was used to track the ZX 12# GEO satellite. The results showed that the ODTT POD accuracy was 3.016 and 2.707 m for 2 and 4 h arcs, respectively. When using both VLBI and ODTT, the POD accuracy was 2.658 m for the 2 h arc, an improvement of 11.87% compared to the POD using ODTT alone. Therefore, VLBI and ODTT can be used together to increase the short-arc POD accuracy while also reducing the arc length necessary to recover the orbit.

Keywords: GEO; POD; ODTT; VLBI

Citation: Nan, K.; Cao, F.; Gong, J.; Lei, H.; Li, Z.; Yang, X. The Short-Arc Precise Orbit Determination of GEO Satellites Using VLBI and Transfer Ranging. *Remote Sens.* **2022**, *14*, 1572. https://doi.org/10.3390/rs14071572

Academic Editors: Shaohui Mei, Xiuping Jia, Ran Tao and Junhui Hou

Received: 20 February 2022
Accepted: 22 March 2022
Published: 24 March 2022

1. Introduction

Geostationary Earth orbit (GEO) satellites play an important role in communication, navigation, positioning, timing, and space engineering [1]. Unlike GPS, GLONASS, and Galileo, which are established based on satellites in the medium Earth orbit, the BeiDou navigation satellite system (BDS) also uses GEO satellites as navigation satellites [2–4]. As GEO satellites must be fixed over the equator, the longitude of the subsatellite point is an important parameter reflecting the position. In order to avoid radio frequency interference and potential collision risk between adjacent satellites, the International Telecommunication Union (ITU) requires that the motion window of a GEO satellite be limited to $\pm 0.1^{\circ}$ in the longitude and latitude directions and ± 50 km in the radial direction [5]. Under the influence of various perturbation factors, there is a long-term drift for a satellite relative to the Earth's fixed position. To maintain a satellite's orbit and for stability of the constellation geometry of the navigation system, the ground monitoring and control system usually makes a maneuver for the satellite at intervals of about 10 days [6]. After the satellite maneuvers, the demand for navigation service can no longer be met by the forecast orbit based on the information of the premaneuver orbit. Therefore, it is critical to rapidly recover the satellite orbit.

Orbit determination by transfer tracking (ODTT) established by the National Time Service Center (NTSC), Chinese Academy of Sciences, is an innovative kind of technology that has high accuracy in the ranging and determination of satellite orbits [7]. At present, it is widely used in the Chinese area positioning system (CAPS) and other C-band transfer ranging (CBTR) systems for precise orbit determination (POD). Due to the use of microwave signals and spread spectrum technology, the ODTT method can achieve a centimeter-level ranging accuracy for high-altitude satellites [8]. Separating the clock offset from the ranging by transfer improves the accuracy of POD at the meter level [9]. ODTT is suitable for the POD of spacecraft in medium and high orbit [10]. However, when the geographical distribution of stations is limited, the geometric structure of satellite observation is poor, and the accuracy of POD in the transverse direction is much worse than in the radial direction. Furthermore, ranging by transfer cannot separate various system errors, such as the delay of the transponder and instruments. In short-arc POD, it is difficult to solve the system errors due to the small amount of data. The above shortcomings can be addressed if joint observation data from ODTT and very long baselines interferometry (VLBI) are used to determine the orbit of GEO satellites.

VLBI was originally invented as an astronomical observation technique back in the 1960s [11]. Due to its high spatial resolution and positioning accuracy, VLBI has been playing an important role in deep space exploration since it was applied to the POD of spacecraft in the 1970s [12–15]. Pseudorange measurement provides range and range rate information on the target in the visual direction, while VLBI provides range and range rate information on the target in the transverse direction. Therefore, VLBI is a natural supplement to pseudorange measurement [16]. When VLBI data is used along with pseudorange measurement data, the orbit positioning accuracy is improved by a factor of 5 [17]. Based on its unique measurement advantages, VLBI can also be applied to high-accuracy observation of artificial earth satellites [18]. System error calibration of the VLBI system can be achieved by observing an extragalactic radio source whose position is precisely known. If the antenna of the VLBI system is very close to that of other ranging systems, the system error of other ranging systems can also be calibrated. For a general range tracking network, the system error is the main source of error in orbit determination. The impact that system errors have can be reduced by adding a small amount of high-accuracy VLBI data [19].

In the 1970s, Kawase and Tanaka [20] used VLBI to observe synchronous satellites. In the 1980s, Tadashi Shiomi utilized differential VLBI and radio ranging to achieve measurement and determination of orbits in synchronous satellites. Shiomi and other scholars [21] used intercontinental differential VLBI data for POD of DSCS-II. In the 21st century, Shu et al. [22] used the Chinese VLBI network for differential VLBI observations of synchronous satellites and successfully obtained satellite interference fringes. Huang et al. [23] used orbital data from the Chinese VLBI network along with C-band transfer ranging to perform joint POD. The orbit determination of GEO satellites was simulated by Du et al. [24] with VLBI data. The result showed that the POD accuracy could be significantly improved by including a small amount of high-accuracy VLBI data. In order to meet the needs of future scientific research, the International VLBI Service for Geodesy and Astrometry (IVS) proposed the VLBI update plan named VLBI 2010 [25–27].

According to the VLBI 2010 specification, the first VLBI 2010 Global Observation System (VGOS) in China was built by NTSC. The system includes a data processing center in Xi'an and three stations in Sanya, Jilin, and Kashi, each of which has an antenna with a diameter of 13 m. The baseline length of Jilin–Kashi, Jilin–Sanya, and Kashi–Sanya is 4081, 3215, and 3900 km, respectively. The distribution of the three baselines helps to enhance the geometric structure of stations for satellite observations. Each station is equipped with a broadband cooling receiver, a broadband recording terminal, and a highly stable hydrogen atomic clock. The broadband cooling receiver is in a dual circular polarization with a frequency coverage of 1.2 to 9 GHz. By cooling the terminal feeder and low-noise amplifier (LNA), the noise temperature of the station system is less than 50 K, which greatly reduces noise and improves the sensitivity of the receiver. The broadband recording terminal can record up to two 16-channel or one 32-channel data. The bandwidth of every channel for recording data is 32 MHz, so the maximum bandwidth of data recording is 1024 MHz. Broadband data is stored in the local disk array in Mark5B format and then transmitted to the Xi'an data processing center through a private network. The Xi'an data processing center has a processing system related to the broadband VLBI hardware, an outline software server, a station monitoring software, a processing cluster related to DiFX [28,29] software, and a related postprocessing software. The experiments on satellites were carried out by the VLBI system in 2017.

Joint observation of ZX #12 GEO satellite was performed by the ODTT and VLBI systems of NTSC. This study investigated the accuracy of short-arc orbit determination using joint ODTT and VLBI observation data.

There are some advantages when VBLI is jointly used with ODTT in POD. Firstly, VLBI is sensitive to the motion of satellites in the transverse direction, while ODTT is sensitive to the motion of satellites in the radial direction. In addition, position dilution of precision (PDOP) can be improved, especially in the transverse direction. Based on these advantages, the accuracy of short-arc POD using VLBI and ODTT is better than that using ODTT alone. Moreover, the arc length used to recover the orbit could become shorter while still ensuring accuracy. This is significant for rapidly recovering the GEO satellite orbit after a maneuver. The rest of the paper is structured as follows. Section 2 introduces the principle of orbit measurement for ODTT and VLBI. Section 3 refers to the improvement on PDOP when VLBI is added to ODTT to observe a satellite, along with some details of the observation. Section 4 presents the results of an experiment based on the measured data. The results indicate that using VLBI and ODTT can not only improve the accuracy of short-arc POD but also rapidly recover the orbit.

2. Principle of Orbit Measurement

VLBI and ODTT measure different parameters to collect orbital data. ODTT provides the radial pseudorange between the satellite and the station, while VLBI provides the time delay of two stations.

2.1. Principle of ODTT

The principle of ODTT is as follows. Using the code division multiple access (CDMA) technology, multiple pseudocode spread spectrum signals can be generated in the same frequency band. Time signals with high accuracy, generated by ground atomic clocks, are broadcast to satellites. The signals are then forwarded to every station by the transponder on the satellite. The distance from the station to the satellite is determined by measuring the path delay of the received signal. There are three observation modes depending on how the signal is transmitted or received: self-transmitting and self-receiving, single-transmitting and multireceiving, and group observation [30]. Among them, the self-transmitting and self-receiving mode can completely eliminate the influence of the atomic clock offset of the ground station. It is the conventional mode for POD of satellites, as shown in Figure 1.

In the Geocentric Terrestrial Reference System (GTRS), self-transmitting and self-receiving observation modes are characterized by a high-accuracy time signal transmitted by the station and forwarded back to the station through the satellite transponder. Under this mode, the accuracy requirement of time synchronization for stations can be satisfied.

Suppose that t_s is the time when station A transmits a signal and t_r is the time when the transmitted signal is received by station A. t is the time when the signal arrives at the satellite and the pseudorange ρ_t at that time is the observation of the station. c is the speed of light in vacuum. Because the satellite signal goes through two processes, up and down, ρ_t is half of the value of the round trip ranging.

$$\begin{cases} t = (t_s + t_r)/2 \\ \rho_t = (t_r - t_s)\ c/2 \end{cases} \tag{1}$$

ρ_t can be expressed as follows:

$$\rho_t = l + \frac{1}{2}(d_t + d_r) + d_{tro} + \frac{1}{2}(d_{ion1} + d_{ion2}) + \frac{1}{2}d_\tau + d_{os} + d_{om} + d_{rl} \tag{2}$$

where 1 is the geometric distance between the station and the satellite at time t, d_t denotes the instrument delay for the station to transmit signals, d_r refers to the instrument delay for the station to receive signals, d_{tro} illustrates the tropospheric delay on the path of propagation, d_{ion1} indicates the ionospheric delay associated with the frequency of the upstream signal, d_{ion2} is the ionospheric delay associated with the frequency of the downstream signal, d_τ denotes the satellite transponder delay, d_{os} refers to the phase center correction of satellite transponder, d_{om} illustrates the phase center correction of the antenna on the ground, and d_{rl} indicates the relativistic effect correction. Measurement models and reference systems are listed in Table 1.

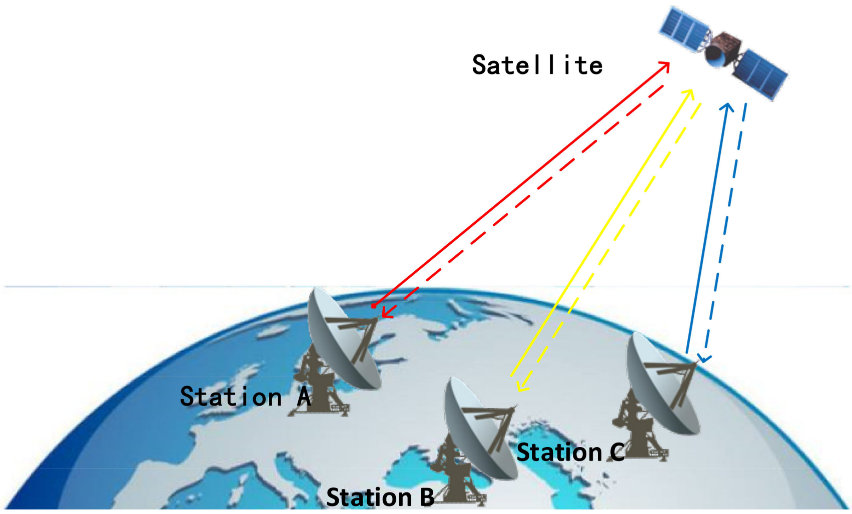

Figure 1. Self-transmitting and self-receiving observation mode.

Table 1. The measurement models and reference systems in orbit determination.

Measurement Models and Reference Systems	Description
The geometric distance	The distance between station and satellite.
The time delay in the station instruments when signal is transmitted and received	The station instruments contain the modem, up/down converters, power amplifier, low noise amplifier, cable, and so on.
The correction of the tropospheric delay	The delay can be corrected by applying the Saastamonien model and the Niell mapping function.
The correction of the ionospheric delay	The delay for ODTT can be calculated by the mean of the uplink and downlink ionospheric delay.
The satellite transponder delay	Though the transponder delay can be measured before satellite transmission, there is still some uncertainty when the satellite is in its orbit.
The antenna phase center correction	The distance from the antenna phase center to the satellite barycenter.
The phase center correction of antenna of the station	The phase center correction of antenna and instrument delay are measured in the first 10 min of every hour when the satellite is observed.
The correction of general relativistic effects	General relativistic effects can be corrected using the Shapiro model.
Reference systems	The inertial J2000.0 system. ITRF2000. The planetary ephemeris DE403/LE403.

2.2. Measuring Principle of VLBI

The basic observation of VLBI is delay and delay rate. The delay of observing extragalactic sources is defined as the time difference between two stations at different positions on the ground when the same signal arrives from the radio source. The change in the delay with time is delay rate. The main part of observation delay (τ_{RSO}) is geometric delay (τ_{RO}), which is determined by the geometrical position of the radio source and the station. The remaining part is the error term (τ_{RSerr}) of the observation delay, including various system errors, such as ionosphere, neutral atmosphere, clock offset, and instrument error as well as random errors in measurement. The relationship between observation delay and geometric delay of the extragalactic radio source is as follows in the International Celestial Reference Frame (ICRF):

$$\tau_{RSO} = \tau_{RO} + \tau_{RSerr} \tag{3}$$

Similarly, the relationship between observation delay (τ_{SPO}), geometric delay (τ_{SP}), and the error term (τ_{SPerr}) of spacecraft is as follows:

$$\tau_{SPO} = \tau_{SP} + \tau_{SPerr} \tag{4}$$

After years of astronomical measurements, the accuracy of the ICRF established with reference to extragalactic radio sources is better than 0.05 arcsecond [31–33], and the angular position measurement accuracy of 295 radio sources in ICRF is better than 10 µas [34–36]. Because the position of the extragalactic radio source is precisely known, the geometric delay of the radio source can be calculated so that the error term can be obtained by the following formula:

$$\tau_{RSerr} = \tau_{RSO} - \tau_{RO} \tag{5}$$

Because the angular position of the spacecraft and that of the radio source are very close, one can assume the following:

$$\tau_{SPerr} \approx \tau_{RSerr} \tag{6}$$

In this way, instrument delay errors, clock offset, and delay errors caused by transmission medium, such as the ionosphere and troposphere, can be effectively removed.

As shown in Figure 2, when the object of observation is a radio source, the distance is nearly an infinite amount compared to the scale of the VLBI baseline. Therefore, it can be considered that the electromagnetic waves received by different antennas are plane waves and that the propagation paths are parallel. Its geometric delay can be written as follows:

$$c\ \tau_{RO} = -B\ I \tag{7}$$

In Equation (7), the baseline vector $B = R_2 - R_1$; $R_i (i = 1, 2)$ is the position vector of the ith station, and I is the unit vector in the direction of the radio source. The geometric delay rate can be obtained as follows:

$$c\ \dot{\tau_{RO}} = -B\ \dot{I} - \dot{B}\ I \tag{8}$$

When the object of observation is a spacecraft, the electromagnetic wave received by different antennas is considered to be a spherical wave rather than a parallel plane wave because spacecraft and stations are relatively close. Its geometric delay can be written as follows:

$$c\ \tau_{SP} = \rho_2 - \rho_1 \tag{9}$$

This is equivalent to differential one-way ranging (DOR) between the spacecraft and two stations. In Equation (9), $\rho_i = \|\vec{\rho_i}\|, \vec{\rho_i} = r - R_i$. $\vec{\rho_i}$ $(i = 1, 2)$ is the slant range vector of the *i*th station, where r is the position vector of the spacecraft. Its geometric delay rate can be written as follows:

$$c\ \dot{\tau_{SP}} = \left(\vec{\rho_{2u}} - \vec{\rho_{1u}}\right)\ \dot{r} + \vec{\rho_{1u}}\ \dot{R_1} - \vec{\rho_{2u}}\ \dot{R_2} \tag{10}$$

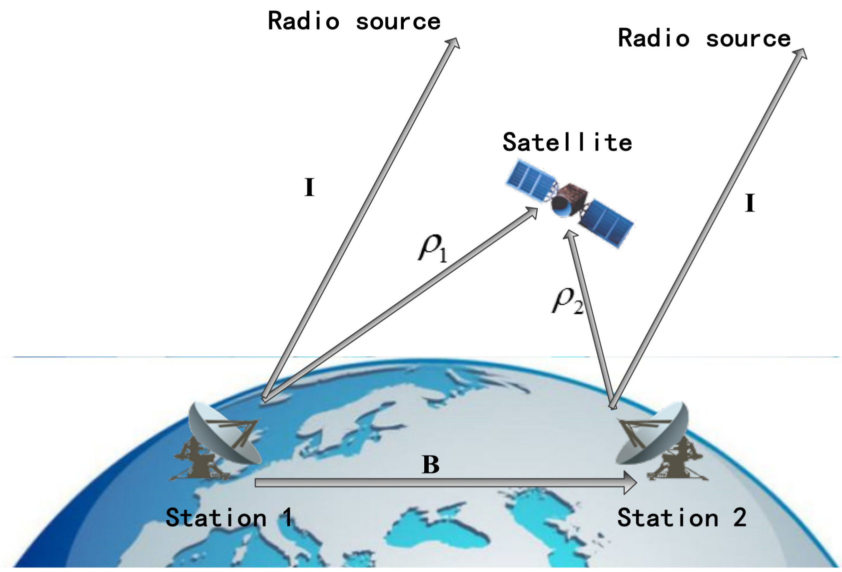

Figure 2. Observation mode of VLBI.

In the above formula, $\vec{\rho}_{iu} = \frac{\vec{\rho}_i}{\rho_i}(i = 1,2)$ is the unit slant range vector of the ith station.

Differential VLBI is used to alternately observe the spacecraft and its nearby extragalactic radio sources. In this way, ΔDOR can be obtained by $c\ \tau_{SPO}$ minus $c\ \tau_{RSO}$:

$$\Delta DOR = c\ (\tau_{SPO} - \tau_{RSO}) \tag{11}$$

From (3), (4), (7), (9), and (11), the following formula can be obtained:

$$\Delta DOR = \rho_2 - \rho_1 + B\ I + c\ \tau_{SRerr} \tag{12}$$

In Equation (12), $\tau_{SRerr} = \tau_{SPerr} - \tau_{RSerr}$; random errors and system errors that are not fully removed are included. Similarly, the delta differential one-way Doppler (ΔDOD) can be written as follows:

$$\Delta DOD = c\ \left(\dot{\tau}_{SPO} - \dot{\tau}_{RSO}\right) \tag{13}$$

From (3), (4), (8), (10), and (13), the following formula can be obtained:

$$\Delta DOD = \left(\vec{\rho}_{2u} - \vec{\rho}_{1u}\right)\ \dot{r} + \left(\vec{\rho}_{1u} - I\right)\ \dot{R}_1 - \left(\vec{\rho}_{2u} - I\right)\ \dot{R}_2 + B\ \dot{I} + c\ \dot{\tau}_{SRerr} \tag{14}$$

When the spacecraft is far enough away from the station the following applies:

$$\vec{\rho}_{1u} \approx \vec{\rho}_{2u} \tag{15}$$

Therefore, Equation (12) can be approximated as follows:

$$\begin{aligned} \Delta DOR &= \rho_2 - \rho_1 + B\ I + c\ \tau_{SRerr} \\ &= \vec{\rho}_2\ \vec{\rho}_{2u} - \vec{\rho}_1\ \vec{\rho}_{1u} + B\ I + c\ \tau_{SRerr} \\ &= \left(\vec{\rho}_1 - \vec{\rho}_2\right)\ \vec{\rho}_{1u} + B\ I + c\ \tau_{SRerr} \\ &= -B\ \left(\vec{\rho}_1 - I\right)\ + c\ \tau_{SRerr} \end{aligned} \tag{16}$$

In Equation (16), $(\vec{\rho}_1 - I)$ represents the angular distance between the spacecraft and the reference radio source. Therefore, the differential VLBI can precisely measure the transverse position and velocity of the target spacecraft.

In the positioning calculation, at least three stations are required to form three baselines to calculate the three components of the position. Having more baselines introduces stronger constraints and leads to more accurate orbit determination.

3. Orbit Measurement Experiment

On 20 August 2017, joint observation of the ZX #12 GEO satellite, with the longitude of the subsatellite point at 87.5°E, was conducted using the ODTT system and the VLBI system. The ODTT system consists of five stations: Changchun station, Xi'an station, Kunming station, Kashi station, and Sanya station. The VLBI system is composed of three baselines: Jilin–Kashi, Jilin–Sanya, and Kashi–Sanya. The distribution of stations is shown in Figure 3.

Figure 3. The distribution of stations.

The influence of the geometric structure of the ground stations on orbit determination of the target satellite can be reflected by PDOP. The distance between the station and the satellite is expanded by Taylor series, and the coefficient matrix through the first-order linearization is as follows:

$$H = \begin{bmatrix} \frac{x_s - x_i}{\rho_i} & \frac{y_s - y_i}{\rho_i} & \frac{z_s - z_i}{\rho_i} \\ \cdots & \cdots & \cdots \\ \cdots & \cdots & \cdots \end{bmatrix} \tag{17}$$

In Equation (17), (x_s, y_s, z_s) is the coordinate of the satellite, (x_i, y_i, z_i) is the coordinate of the *i*th station; ρ_i is the distance between the satellite and the *i*th station. When the VLBI baseline is added, the coefficient matrix becomes the following:

$$H = \begin{bmatrix} \frac{x_s - x_{i1}}{\rho_{i1}} - \frac{x_s - x_{i2}}{\rho_{i2}} & \frac{y_s - y_{i1}}{\rho_{i1}} - \frac{y_s - y_{i2}}{\rho_{i2}} & \frac{z_s - z_{i1}}{\rho_{i1}} - \frac{z_s - z_{i2}}{\rho_{i2}} \\ \cdots & \cdots & \cdots \\ \cdots & \cdots & \cdots \end{bmatrix} \tag{18}$$

In Equation (18), $\left(x_{ij}, y_{ij}, z_{ij}\right)$ is the coordinate of the *j*th (*j* = 1, 2) station in the *i*th baseline. PODP can then be calculated by the following formula:

$$\left(H^T H\right)^{-1} = \begin{bmatrix} D_{11} & D_{12} & D_{13} \\ D_{21} & D_{22} & D_{23} \\ D_{31} & D_{32} & D_{33} \end{bmatrix} \tag{19}$$

$$\mathrm{PDOP} = \sqrt{\mathrm{D}_{11} + \mathrm{D}_{22} + \mathrm{D}_{33}} \tag{20}$$

From (17)–(20), the PDOP value of the geometric structure formed with the ODTT system and the ZX #12 GEO satellite is 25.12. By adding two VLBI baselines, the PDOP value decreases to 15.35. A large reduction in PDOP value suggests that VLBI baselines are beneficial to improve the quality of satellite observations.

The spatial position of a satellite can be decomposed into three orthogonal components: radial direction, tangential direction, and normal direction. The transverse direction is the combination of the tangential and the normal directions. In order to reflect the contribution of PDOP in the transverse direction of the satellite orbit, a local coordinate system needs to be built on the basis of the Earth-fixed coordinate system. In the local coordinate system, the X axis points to the subsatellite point through rotation. The new station coordinates need to be obtained by multiplying the following matrix A by the original coordinate:

$$\mathrm{A} = \begin{bmatrix} cos\theta_{\mathrm{s}} & sin\theta_{\mathrm{s}} & 0 \\ -sin\theta_{\mathrm{s}} & cos\theta_{\mathrm{s}} & 0 \\ 0 & 0 & 1 \end{bmatrix} \tag{21}$$

In Equation (21), θ_s is the longitude of the subsatellite point.

The new satellite coordinate (newco) is as follows:

$$\mathrm{newco} = (\mathrm{R}\;0\;0) \tag{22}$$

where R is obtained by the following equation:

$$\mathrm{R} = \sqrt{\mathrm{x}_{\mathrm{s}}^2 + \mathrm{y}_{\mathrm{s}}^2 + \mathrm{z}_{\mathrm{s}}^2} \tag{23}$$

Substituting the new coordinate into Formulas (17)–(19), a new matrix P can be obtained as follows:

$$\mathrm{P} = \begin{bmatrix} \mathrm{D}_{11}^* & \mathrm{D}_{12}^* & \mathrm{D}_{13}^* \\ \mathrm{D}_{21}^* & \mathrm{D}_{22}^* & \mathrm{D}_{23}^* \\ \mathrm{D}_{31}^* & \mathrm{D}_{32}^* & \mathrm{D}_{33}^* \end{bmatrix} \tag{24}$$

PDOP in the radial direction can be obtained as follows:

$$\mathrm{PDOP}_{\mathrm{r}} = \sqrt{\mathrm{D}_{11}^*} \tag{25}$$

PDOP in the transverse direction can be obtained as follows:

$$\mathrm{PDOP}_{\mathrm{t}} = \sqrt{\mathrm{D}_{22}^* + \mathrm{D}_{33}^*} \tag{26}$$

PDOP was recalculated with the local coordinates, and the result is shown in Table 2.

Table 2. PDOP in different directions of the satellite.

System	Radial Direction (m)	Transverse Direction (m)
ODTT	2.15	25.04
ODTT + VLBI	1.36	15.29

As can be seen, PDOP in the radial direction decreased from 2.15 to 1.36, while PDOP in the transverse direction decreased from 25.04 to 15.29. Thus, it can be seen that the improvement of PDOP is mainly reflected in the transverse direction.

The ODTT system observes the satellite using the self-transmitting and self-receiving mode with a code rate of 20 Mbps and a sampling interval of 1 s. The measurement accuracy can reach centimeter level. The VLBI system alternately observes the satellite and the radio source. The signal of a radio source is weak. To ensure sufficient signal-to-noise ratio, data recording needs 16 channels with a bandwidth of 512 MHz when the target is a radio source.

The signal of a satellite is strong, and its bandwidth is narrow. Data recording just needs one channel with a bandwidth of 32 MHz when the target is a satellite. In each period of alternating observation, the observation time is 50 s for the radio source, 10 s for the satellite, and 10 s for the rotating antenna. The data sampling rate of the VLBI system is 10 s. The geodetic VLBI usually takes group delay as its observation. Due to the limitation of various conditions, the signal bandwidth is generally less than 10 MHz, and the measurement accuracy of group delay is limited to the order of nanoseconds. GEO satellites have a wide bandwidth and a strong signal-to-noise ratio, so a group delay measurement accuracy better than 1 ns can be achieved with a broadband VLBI system [18].

When observing different targets, the observation strategy needs to be adjusted accordingly. It is necessary to reconsider the delay model, reduce the antenna gain, and control the antenna rotation according to the characteristics of the satellite. The theoretical time delay of a radio source is calculated by a far-field model, which is not suitable for satellites and needs to be changed to a near-field model. The signal strength of satellites is much stronger than that of a radio source, which can easily lead to power saturation and signal distortion in the antenna system. Therefore, it is necessary to design the antenna gain system as a two-stage amplifier. The primary amplifier is used for observing the satellite, while the primary and secondary amplifiers are used for observing the radio source. The outline of the radio source observation is not suitable for satellites. In order to ensure correct pointing of the antenna during satellite observation, it is necessary to control the antenna by means of orbit guidance.

It is necessary to select a suitable radio source for alternate observation with satellites. Because the system was built recently, radio sources with fringes obtained in previous experiments should have more than 1 Jy in the C-band. Furthermore, the angular difference between the radio source and the ZX #12 GEO satellite mapping in the celestial coordinate system is required to remain within 10°. Radio sources selected in the experiment are shown in Table 3.

Table 3. Information on radio sources.

Radio Source	Right Ascension (hhmmss)	Declination (ddmmss)	Flow (Jy)
0003−066	00 06 13.892890	−06 23 35.33529	1.38
0106+016	01 08 38.771110	+01 35 00.31725	1.31
0420−014	04 23 15.800724	−01 20 33.06553	2.11
0605−085	06 07 59.699234	−08 34 49.97815	1.50
0742+103	07 45 33.059522	+10 11 12.69226	1.11
1055+018	10 58 29.605207	+01 33 58.82365	1.48
3C273B	12 29 06.699731	+02 03 08.59803	3.49
1510−089	15 12 50.532931	−09 05 59.82986	0.50
1741−038	17 43 58.856136	−03 50 04.61657	2.29
2008−159	20 11 15.710930	−15 46 40.25370	1.35
2134+00	21 36 38.586327	+00 41 54.21275	2.32

The radio sources above all meet the flow density above 1 Jy except 1510-089 and have angular distance from the satellite within 10°, which can cover the entire observation.

4. Precise Orbit Determination Experiment

GEO satellites need frequent maneuvers in order to maintain fixed orbital positions. The forecast orbit based on the information of the premaneuver orbit is very different from the actual orbit after maneuvering, from several kilometers to even tens of kilometers. Short-arc orbit determination is usually used after maneuvering to quickly recover the satellite orbit.

4.1. Improving the Accuracy of Short-Arc Orbit Determination

Based on the joint observation of the ODTT system and the VLBI system, an experiment on short-arc orbit determination was conducted. The satellite was the ZX #12 GEO, and the data for orbit determination was from 13:00 on 20 August 2017 to 07:00 on 21 August 2017. A batch processor was used to run the data [2]. Figure 4 shows the difference in VLBI data compared to the long-arc orbit data. The numbers from 12 to 24 in abscissa belong to 20 August. After number 24, the time in abscissa belongs to the next day, so number 26 actually represents 02:00 on 21 August. The value in ordinate represents the residual of VLBI data, and the range of −1.0 to 1.0 m meets the demand of POD in general. However, there is an area "C" in the middle of Figure 4. The residual of two baselines, namely Jilin–Kashi and Jilin–Sanya, has a large fluctuation that could influence the POD in this arc.

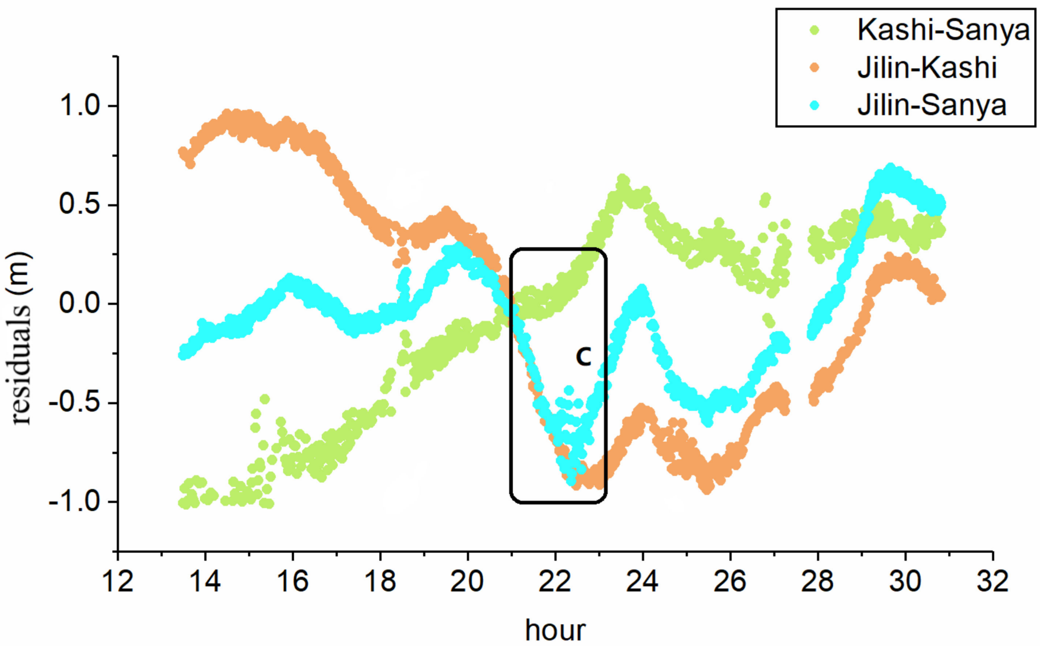

Figure 4. The result of checking VLBI data with long-arc orbit determination.

In the short-arc orbit determination, some parameters are not solved, such as the system error caused by the ionosphere, neutral atmosphere, clock offset, and instrument, which are not fully removed, as well as the solar radiation pressure coefficient and the T-direction empirical acceleration. These parameters were fixed with the values solved in the joint long-arc orbit determination. Thus, the unknowns that needed to be solved in short-arc orbit determination were only the position and velocity of the satellite. The same strategy was used in POD with ODTT data and POD with joint data including ODTT and VLBI. The only difference between two kinds of POD was the data used.

There were nine arcs in total, with each arc lasting 2 h. Figures 5 and 6 show the residuals of five stations belonging to the ODTT system and three baselines belonging to the VLBI system, respectively, when the arc was from 17:00 to 19:00 on 20 August 2017. The average residual was 0.138 m for the ODTT system and0.239 m for the VLBI system. Considering that the measurement accuracy of VLBI is not as good as ODTT, this result is acceptable.

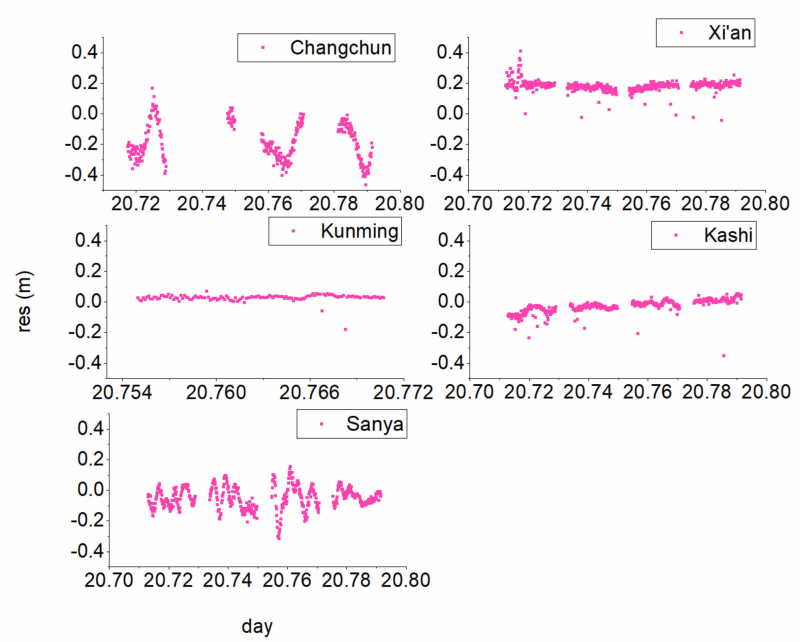

Figure 5. The residuals of five stations of the ODTT system.

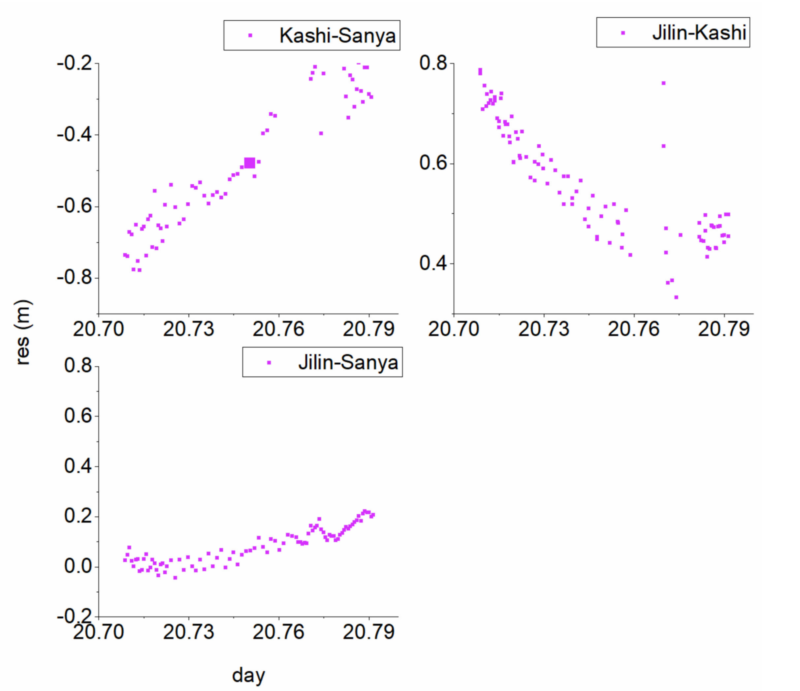

Figure 6. The residuals of three baselines of the VLBI system.

The length of the arc was 2 h. In this condition, the parameters to be solved were only position and velocity. The system errors could not be removed and were absorbed in POD, which could have led to linear or quadratic trends in the plots of Figures 5 and 6.

Considering that a long-arc orbit determined by ODTT and VLBI is more accurate than by ODTT alone [18], the long-arc orbit determined by ODTT and VLBI can be taken as the standard orbit to evaluate the accuracy of the short-arc orbit determined by ODTT and VLBI and by ODTT alone. The length of each short arc was 2 h. The standard orbit had an arc of 18 h, which covered the whole period of observation. The results are shown in Table 4.

Table 4. The results of the bias with arcs of 2 h.

Arc	2 h Orbit Determination by ODTT (m)				2 h Orbit Determination by ODTT and VLBI (m)				Improvement
	R	T	N	Pos	R	T	N	Pos	
20 August 13:00–20 August 15:00	0.245	0.097	4.113	4.122	0.192	0.094	3.567	3.574	
20 August 15:00–20 August 17:00	0.200	0.572	2.549	2.620	0.180	0.701	2.248	2.362	
20 August 17:00–20 August 19:00	0.122	1.082	2.362	2.601	0.091	0.895	2.089	2.274	
20 August 19:00–20 August 21:00	0.408	2.742	4.076	4.930	0.313	2.361	3.145	3.946	
20 August 21:00–20 August 23:00	0.381	2.544	2.878	3.860	0.455	2.811	3.597	4.588	
20 August 23:00–21 August 01:00	0.133	1.445	1.374	1.999	0.078	1.087	0.822	1.365	
21 August 01:00–21 August 03:00	0.193	2.426	1.124	2.681	0.116	2.021	1.070	2.290	
21 August 03:00–21 August 05:00	0.198	1.132	1.428	1.834	0.175	1.042	1.180	1.584	
21 August 05:00–21 August 07:00	0.213	0.663	2.402	2.501	0.168	1.271	1.464	1.947	
Average				3.016				2.658	11.87%

The long-arc orbit was taken as the standard orbit to evaluate the short-arc orbit. The accuracy is reflected from four aspects: radial direction, tangential direction, normal direction, and spatial position. The table gives the results of the bias in nine arcs. R represents the radial direction, T represents the tangential direction, N represents the normal direction, and Pos represents the spatial position. The bias from the ODTT and VLBI test case was smaller compared to the one for ODTT alone. The bias become worse only in the arc 20 August 21:00–20 August 23:00. The preliminary inference was that this was due to the instability of the clock in Jilin station during this period. Considering the Jilin–Kashi and Jilin–Sanya baselines yield a large fluctuation during 21:00–23:00, it may explain the worse bias of this 2 h arc (see Figure 4). From a statistical point of view, the average position bias of the nine arcs decreased from 3.016 to 2.658 m, and the POD accuracy improved by 11.87%. When the abnormal arc with the worse bias was eliminated, the average position bias of the eight arcs decreased from 2.911 to 2.418 m, and the accuracy of orbit determination improved by 16.94%.

Table 5 shows results for an arc length of 1.5 h.

Table 5. The results of the bias with arcs of 1.5 h.

Arc	1.5 h Orbit Determination by ODTT (m)				1.5 h Orbit Determination byODTT and VLBI (m)				Improvement
	R	T	N	Pos	R	T	N	Pos	
20 August 13:00–20 August 14:30	0.234	0.175	4.066	4.076	0.191	0.219	3.628	3.639	
20 August 14:30–20 August 16:00	0.303	1.030	3.886	4.031	0.245	1.018	3.205	3.372	
20 August 16:00–20 August 17:30	0.076	0.426	1.477	1.539	0.072	0.228	1.406	1.426	
20 August 17:30–20 August 19:00	0.138	1.069	2.447	2.674	0.103	0.916	2.111	2.303	
20 August 19:00–20 August 20:30	0.351	2.352	3.757	4.447	0.241	1.921	2.670	3.298	
20 August 20:30–20 August 22:00	0.481	3.205	4.051	5.189	0.464	3.166	3.8552	5.010	
20 August 22:00–20 August 23:30	0.225	1.170	1.386	1.828	0.374	1.737	2.883	3.387	
20 August 23:30–21 August 01:00	0.164	1.726	1.548	2.325	0.106	1.431	1.016	1.759	
21 August 01:00–21 August 02:30	0.182	2.838	0.712	2.932	0.077	2.391	0.872	2.547	
21 August 02:30–21 August 04:00	0.220	1.036	1.803	2.092	0.166	0.858	1.277	1.548	
21 August 04:00–21 August 05:30	0.134	1.155	1.016	1.544	0.174	1.323	1.023	1.682	
21 August 05:30–21 August 07:00	0.245	0.622	2.659	2.741	0.186	1.221	1.883	2.252	
Average				2.951				2.685	9.01%

Table 6 shows the results for an arc length of 1 h.

Table 6. The results of bias with arcs of 1 h.

Arc	1 h Orbit Determination by ODTT (m)				1 h Orbit Determination by ODTT and VLBI (m)				Improvement
	R	T	N	Pos	R	T	N	Pos	
20 August 13:00–20 August 14:00	0.249	0.131	4.139	4.148	0.199	0.119	3.584	3.592	
20 August 14:00–20 August 15:00	0.244	0.041	4.122	4.129	0.181	0.078	3.470	3.476	
20 August 15:00–20 August 16:00	0.305	1.291	3.560	3.799	0.268	1.336	3.088	3.375	
20 August 16:00–20 August 17:00	0.118	0.436	1.637	1.698	0.117	0.424	1.539	1.601	
20 August 17:00–20 August 18:00	0.111	0.271	1.430	1.459	0.099	0.191	1.321	1.338	
20 August 18:00–20 August 19:00	0.242	1.875	3.587	4.055	0.188	1.658	3.085	3.508	
20 August 19:00–20 August 20:00	0.343	2.225	3.846	4.456	0.218	1.720	2.615	3.138	
20 August 20:00–20 August 21:00	0.464	3.073	4.141	5.177	0.404	2.857	3.590	4.606	
20 August 21:00–20 August 22:00	0.398	2.800	2.982	4.110	0.417	2.849	3.167	4.281	
20 August 22:00–20 August 23:00	0.321	1.871	2.727	3.323	0.476	2.559	3.805	4.610	
20 August 23:00–21 August 00:00	0.070	1.078	1.126	1.560	0.079	0.697	0.609	0.930	
21 August 00:00–21 August 01:00	0.245	1.593	2.736	3.176	0.182	1.368	2.165	2.568	
21 August 01:00–21 August 02:00	0.184	2.885	0.947	3.042	0.083	2.373	1.206	2.663	
21 August 02:00–21 August 03:00	0.189	1.917	1.382	2.371	0.132	1.616	1.344	2.106	
21 August 03:00–21 August 04:00	0.224	0.984	1.784	2.050	0.181	0.840	1.377	1.623	
21 August 04:00–21 August 05:00	0.161	1.317	0.870	1.587	0.167	1.275	0.940	1.593	
21 August 05:00–21 August 06:00	0.108	0.756	1.532	1.712	0.199	1.441	1.436	2.044	
21 August 06:00–21 August 07:00	0.291	0.560	3.093	3.157	0.178	1.076	1.966	2.248	
Average				3.056				2.738	10.40%

The POD accuracy improved by 11.87% with arcs of 2 h, 9.01% with arcs of 1.5 h, and 10.40% with arcs of 1 h. This indicates that the POD accuracy with short arcs is improved when the joint orbit determination technique is used.

Table 4, Table 5, and Table 6 give the bias in three directions: normal, tangential, and radial. As mentioned in Section 3, the transverse direction is the combination of the tangential and the normal directions. In order to reflect the contribution of VLBI in the transverse direction of the orbit, the bias in the transverse direction and radial direction is shown in Figure 7.

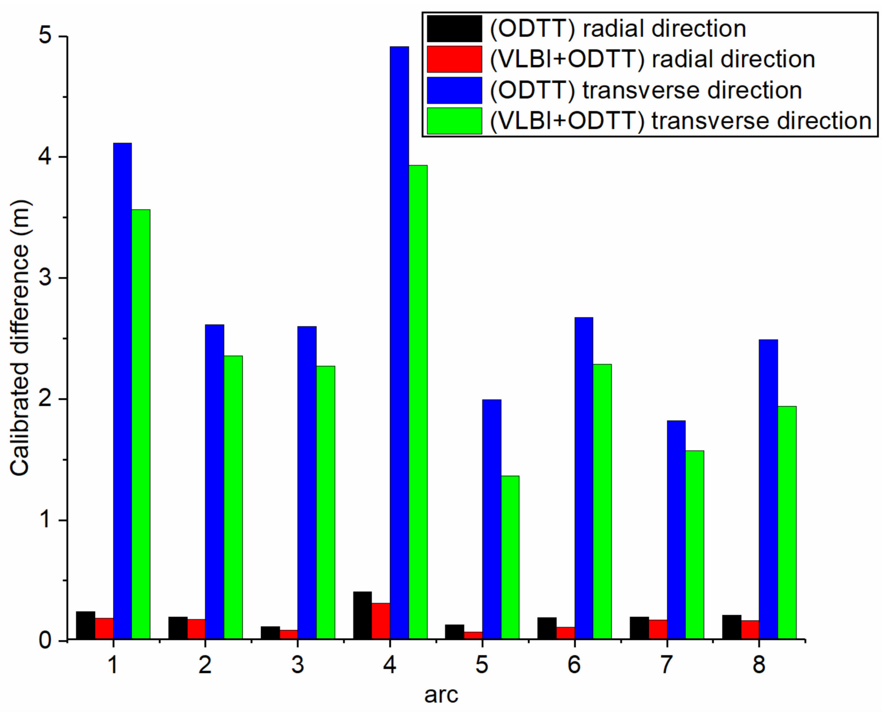

Figure 7. The bias in the transverse and radial direction.

The figure shows the bias of the eight arcs in the transverse and radial directions except the abnormal arc when the time for the arc was 2 h. Through joint orbit determination by ODTT and VLBI, the improvement of the transverse bias was better than that of the radial bias. The average bias in the radial direction decreased from 0.214 to 0.164 m, representing an improvement of 0.050 m. The average bias in the transverse direction decreased from 2.902 to 2.411 m, representing an improvement of 0.491 m. The improvement along the transverse direction was about 10 times that of the radial direction.

There were nine arcs in total when each arc had the length of 2 h. As it is not necessary to give the continuous bias of all arcs, Figures 8 and 9 show the continuous bias of two arcs that were randomly selected.

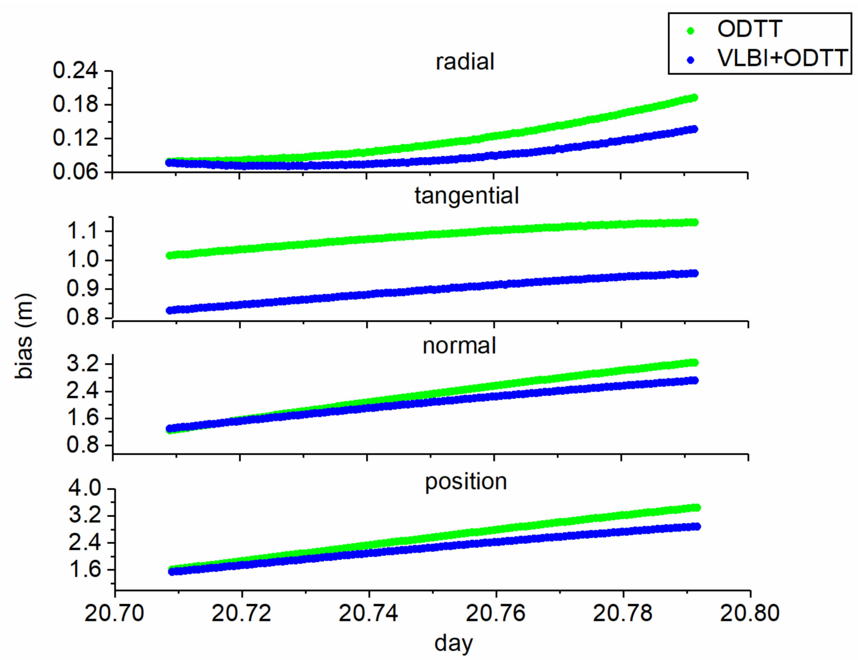

Figure 8. The bias during the period of 20 August 17:00–20 August 19:00.

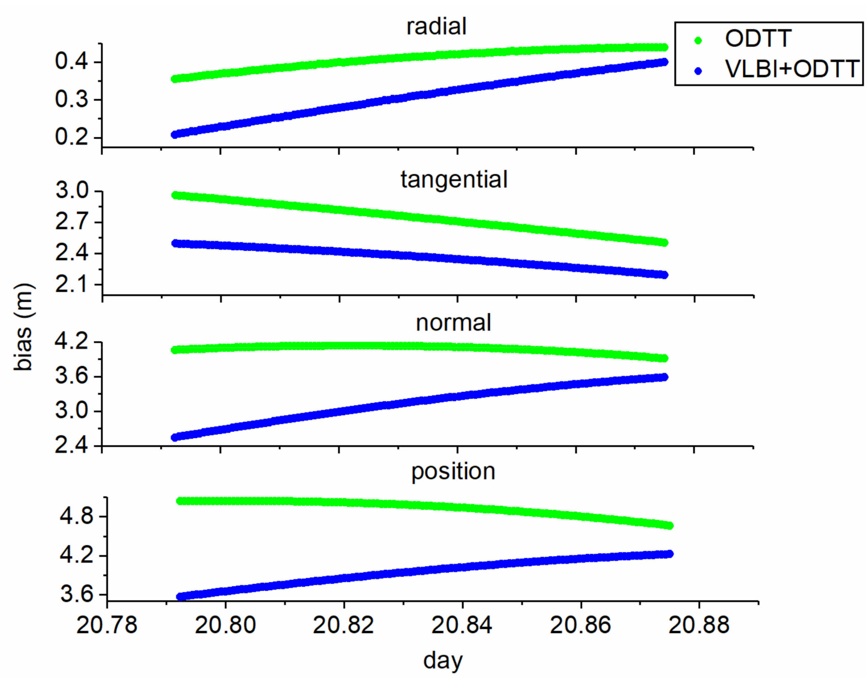

Figure 9. The bias during the period of 20 August 19:00–20 August 21:00.

From Figures 8 and 9, it can be seen that the bias by ODTT and VLBI was smaller than that by ODTT alone. Therefore, the accuracy was improved. Although the bias was improved in the radial direction, it was not as significant as the improvement in the tangential and the normal directions.

4.2. Improving the Efficiency of Orbital Recovery

The results of short-arc orbit determination by ODTT were obtained with arc lengths of 3, 4, and 5 h.

Figure 10 shows the average bias in position with different arc lengths. A1, A2, and A3 represent the average value of joint orbit by ODTT and VLBI when each arc was 1, 1.5, and 2 h, respectively. B1, B2, B3, and B4 represent the average value of orbit by ODTT alone when each arc was 2, 3, 4, and 5 h.

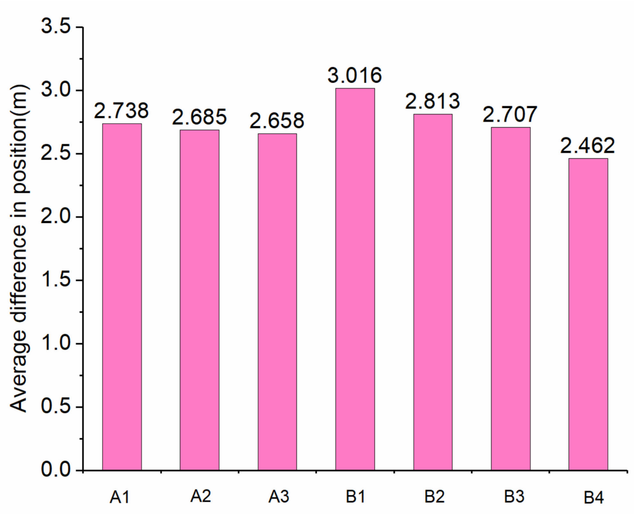

Figure 10. The difference in position with different kinds of orbit determination and arc length.

As can be seen from Figure 10, the bias of the 1 h joint orbit determination by ODTT and VLBI was 2.738 m. The bias for 2 and 3 h orbit determination by ODTT alone was 3.016 and 2.813 m, respectively. Therefore, the bias of the 1 h joint orbit determination by ODTT and VLBI was better than the 2 and 3 h ones by ODTT alone. The average bias of the 4 h orbit by ODTT was 2.707 m, which was the same approximate accuracy as the 1 h joint orbit determination by ODTT and VLBI but took 4 times as long. In addition, the accuracy of the 2 h joint orbit determination by ODTT and VLBI was 2.658 m, while that of ODTT was 3.016 m. Obviously, the accuracy of ODTT and VLBI was better than that of ODTT when the length of the arc was the same. This proves that joint orbit determination by ODTT and VLBI improves not only the accuracy but also the orbit recovery efficiency.

5. Summary

Based on the ODTT and VLBI of NTSC of Chinese Academy of Sciences, joint observation of the ZX #12 GEO satellite was conducted. ODTT can achieve high accuracy in the radial direction but is weak in the transverse direction, while VLBI can achieve high accuracy in the transverse direction, making the two methods complementary. VLBI can calibrate its own system error by observing an extragalactic radio source whose position is precisely known, so its measurement accuracy can meet the requirement. Furthermore, PDOP can be reduced, especially in the transverse direction, when VLBI and ODTT conduct joint observation of satellites. In our study, the value of PDOP decreased from 2.15 to 1.36 in the radial direction and from 25.04 to 15.04 in the transverse direction. Based on these advantages of LVBI, the accuracy of short-arc POD using VLBI and ODTT could be improved.

The experiment showed that the accuracy of short-arc orbit improved by 11.87% when each arc was 2 h. The average bias in the radial direction decreased from 0.214 to 0.164 m, representing an improvement of 0.050 m, while the average bias in the transverse direction decreased from 2.902 to 2.411 m, representing an improvement of 0.491 m. Therefore, the accuracy of POD can be obviously improved by integrating VLBI and ODTT data, especially in the transverse direction.

The accuracy of the 1 h joint orbit determination using both ODTT and VLBI was 2.738 m, while the accuracy of 4 h orbit determination by ODTT alone was 2.707 m. Although the accuracy was approximate, joint POD using both ODTT and VLBI saved 4 times the time. It was also proven that the orbit could be recovered faster by integrating VLBI and ODTT data, which has a great role in GEO as it needs to make frequent maneuvers.

In short, using VLBI and ODTT together could not only improve the accuracy of short-arc POD but also rapidly recover the orbit.

Author Contributions: K.N. performed the main data analysis and wrote the original draft; F.C. performed parts of the experiments with constructive discussion and contributed to language editing; H.L. and J.G. performed parts of the experiments and contributed to language editing; Z.L. contributed to constructive comments; X.Y. contributed to constructive comments. All authors have read and agreed to the published version of the manuscript.

Funding: This work was supported by the National Natural Science Foundation of China (No. 41604026, No. 11703033, No. 12073034), Natural Science Foundation of Shaanxi (No. 20190398), Youth Promotion Committee of Chinese Academy of Sciences, and 100 Talents Project of the Chinese Academy of Sciences, CAS "Light of West China" Program (No. XAB2019A06, No. XAB2018YDYL01).

Institutional Review Board Statement: Not applicable.

Informed Consent Statement: Not applicable.

Data Availability Statement: The ODTT and VLBI data used in this work were provided by the NTSC.

Acknowledgments: The authors would like to thank the support from the International GNSS Monitoring and Assessment system (iGMAS), the iGMAS analysis center at NTSC.

Conflicts of Interest: The authors declare no conflict of interest.

References

1. Li, Z.; Yang, X.; Shi, C.; Ge, Y. A new method for determination of satellite orbits by transfer. *Sci. China Ser. G* **2008**, *38*, 1711–1722.
2. Fen, C.; XuHai, Y.; Zhigang, L.; ChuGang, F. POD experiments using real and simulated time-sharing observations for GEO satellites in C-band transfer ranging system. *Adv. Space Res.* **2016**, *58*, 488–497. [CrossRef]
3. Ye, F.; Yuan, Y.; Ou, J. Initial orbit determination of BDS-3 satellites based on new code signals. *Geod. Geodyn.* **2018**, *9*, 342–346. [CrossRef]
4. Manzino, A.M.; Dabove, P.; Gogoi, N. Assessment of positioning performances in Italy from GPS, BDS and GLONASS constellations. *Geod. Geodyn.* **2018**, *9*, 439–448. [CrossRef]
5. Huang, Y.; Hu, X.; Huang, C.; Yang, Q. Using CAPS ranging data to determine the orbit of GEO satellite during orbital change. *Sci. China Ser. G* **2008**, *38*, 1750–1758.
6. Guo, R.; Zhou, J.; Hu, X.; Liu, L. A Strategy of Rapid Orbit Recovery for the Geo Stationary Satellite. *Acta Geod. Cartogr. Sin.* **2011**, *40*, 19–25.
7. Cao, F. Research on Precise Orbit Determination by Transfer for GEO Navigation Satellites. Ph.D. Thesis, The University of Chinese Academy of Sciences, Beijing, China, 2014.
8. Yang, X.; Ding, S.; Lei, H.; Cao, F. Research progress of the technology of orbit observation and determination via transfer. *J. Time Freq.* **2016**, *39*, 216–224. [CrossRef]
9. Nan, K.; Yang, X.; Cao, F.; Zhang, J. Orbit determination by transfer tracking based on high-precise tropospheric delay correction. *J. Time Freq.* **2018**, *41*, 56–65. [CrossRef]
10. Lei, H. Research on Precise Orbit Determination of Navigation Satellites Based on Transponder Ranging. Ph.D. Thesis, The University of Chinese Academy of Sciences, Beijing, China, 2011.
11. Xia, J.; Li, J.; Han, Y. On the Next Generation of the VLBI System-VLBI2010. *Prog. Geophys.* **2010**, *25*, 1623–1627. [CrossRef]
12. Antreasian, P.G.; Baird, D.T.; Border, J.S.; Burckhart, P.D.; Graat, E.J.; Jah, M.K.; Mase, R.A.; McElrath, T.P.; Portock, B.M. 2001 Mars Odyssey Orbit Determination During Interplanetary Cruise. *J. Spacecr. Rocket.* **2005**, *42*, 394–405. [CrossRef]

13. Border, J.; Donivan, F.; Finley, S. Determining spacecraft angular position with Delta VLBI-The Voyager demonstration. In Proceedings of the Astrodynamics Conference, San Diego, CA, USA, 9–11 August 1982.
14. Kroger, P.; Folkner, W.; Iijima, B. Very long baseline interferometry measurements of planetary orbiters at Mars and Venus. In Proceedings of the AIAA Spaceflight Mechanics Meeting, Pasadena, CA, USA, 22–24 February 1993; Volume 95.
15. Pogrebenko, S.; Gurvits, L.; Campbell, R. VLBI tracking of the Huygens probe in the atmosphere of Titan. *Planet. Probe Atmos. Entry Descent Trajectory Anal. Sci.* **2004**, *544*, 197–204.
16. Berry, D.; Border, J. *CCSDS Concept Paper Delta-DOR*; NASA: Washington, DC, USA, 2005.
17. Thornton, C.; Border, J. *Radiometric Tracking Techniques for Deep Space Navigation*; Jet Propulsion Laboratory Publication: Pasadena, CA, USA, 2003.
18. Gong, J.; Cao, F.; Yang, X.; Li, Z. The GEO Satellite Orbit Experiment Measured by Combination of the Broadband VLBI & the Orbit Tracking of Two Way Range. *Bol. Tec./Tech. Bull.* **2017**, *55*, 39–47.
19. Du, L. A Study on the Precise Orbit Determination of Geostationary Satellites. Ph.D. Thesis, Information Engineering University, Zhengzhou, China, 2006.
20. Kawase, S.; Tanaka, T. Oribt determination of a geosynchronous satellite by the VLBI technique. *J. Radio Res. Lab.* **1978**, *26*, 65–71.
21. Shiomi, T.; Kawano, N. Precise orbit determination of a geosynchronous satellite by VLBI. *J. Jpn. Soc. Aeronaut. Space Sci.* **1987**, *35*, 425–432. [CrossRef]
22. Shu, F.; Zhang, X.; Zheng, W. VLBI Observations of Geosynchronous Satellites. *Ann. Shanghai Obs. Acad. Sin.* **2003**, *24*, 105–111.
23. Huang, Y.; Hu, X.; Zhang, X.; Jiang, D. Application of VLBI in Orbit Determination of GEO Navigation Satellite. *Sci. China* **2011**, *56*, 1974–1981.
24. Du, L.; Zheng, Y.; Li, J. VLBI augmented Orbit Determination for Geostationary Satellites. *J. Zhengzhou Inst. Surv.* **2006**, *23*. Available online: https://xueshu.baidu.com/usercenter/paper/show?paperid=7839061746bde43a6178240cf2f284c7&site=xueshu_se (accessed on 10 February 2022).
25. Behrend, J.; Boehm, J.; Charlot, P.; Nan, K. *Recent Progress in the VLBI2010 Development*; Observing Our Changing Earth; Springer: Berlin/Heidelberg, Germany, 2008.
26. Niell, A.; Whitney, A.; Petrachenko, W.; Schlüter, W.; Vandenberg, N.; Hase, H.; Koyama, Y.; Ma, C.; Schuh, H.; Tuccari, G. VLBI2010: A Vision for Future Geodetic VLBI. In *Dynamic Planet*; Springer: Berlin/Heidelberg, Germany, 2007.
27. Petrachenko, B.; Behrend, D.; Gipson, J.; Hase, H.; Ma, C.; Macmillan, D.; Niell, A.; Nothnagel, A.; Zhang, X. VGOS Observing Plan. In *International VLBI Service for Geodesy and Astrometry 2014 General*; Armstrong, Science Press: Beijing, China, 2014; pp. 16–19. ISBN 978-7-03-042974-2.
28. Deller, A.; Brisken, W.F.; Phillips, C.; Morgan, J.; Alef, W.; Cappallo, R.; Middelberg, E.; Romney, J.; Rottmann, H.; Tingay, S.J.; et al. DiFX-2: A More Flexible, Efficient, Robust, and Powerful Software Correlator. *Publ. Astron. Soc. Pac.* **2011**, *123*, 275–287. [CrossRef]
29. Deller, A.T.; Tingay, S.; Bailes, M.; West, C. DiFX: A Software Correlator for Very Long Baseline Interferometry Using Multiprocessor Computing Environments. *Publ. Astron. Soc. Pac.* **2007**, *119*, 318–336. [CrossRef]
30. Cao, F.; Yang, X.; Li, Z.; Liang, C.; Feng, C. Signal Biases Calibration for Precise Orbit Determination of the Chinese Area Positioning System using SLR and C-Band Transfer Ranging Observations. *J. Navig.* **2016**, *69*, 1234–1246.
31. Feissel, M.; Mignard, F. The adoption of ICRS on 1 January 1998: Meaning and consequences. *Astron. Astrophys.* **1998**, *331*, L33–L36.
32. Ma, C.; Arias, E.F.; Eubanks, T.M.; Fey, A.L.; Gontier, A.M.; Jacobs, C.S.; Sovers, O.J.; Archinal, B.A.; Charlot, P. The International Celestial Reference Frame realized by VLBI. *IERS Tech. Note* **1997**, *23*, II-1–II-44.
33. Treuhaft, R.N. Deep Space Tracking in Local Reference Frames. In *Telecommunications & Data Acquisition Progress Report*; NASA: Washington, DC, USA, 1988; Volume 94.
34. Gerard, P.; Brian, L. *IERS Conventions (2010)*; IERS Conventions Centre: Frankfurt am Main, Germany, 2010.
35. Hong, X. VLBI Technique and Application in the Change Lunar Orbit. *Chin. J. Nat.* **2007**, *29*, 297–299. [CrossRef]
36. Zhu, X.; Li, C.; Zhang, H. A Survey of VLBI Technique for Deep Space Exploration and Trend in China Current Situation and Development. *J. Astronaut.* **2010**, *31*, 1893–1899. [CrossRef]